Incorporation of Fe into the void corner of the incomplete cubane-type $Ir_3S(SH)_3$ sulfido-hydrosulfido cluster to give new cubane-type Ir_3FeS_4 clusters

Hidetake Seino, Hiroyuki Mori, Aya Shinozaki, Yasushi Mizobe*

Institute of Industrial Science, The University of Tokyo, Komaba, Meguro-ku, Tokyo 153-8505, Japan

ABSTRACT

Treatment of incomplete cubane-type cluster $[(Cp^*Ir)_3(\mu_3\text{-}S)(\mu_2\text{-}SH)_3]Cl$ (**1**; $Cp^* = \eta^5\text{-}C_5Me_5$) with $FeCl_2$ in the presence of excess NEt_3 afforded a cationic cubane-type cluster $[(Cp^*Ir)_3(FeCl)(\mu_3\text{-}S)_4][FeCl_2(\mu\text{-}Cl)_2FeCl_2]_{0.5}$ (**4**), although isolation of **4** as pure crystals was somehow unable to be reproduced. On the other hand, reaction of **1** with $FeCl_3$ or $Fe(BF_4)_2 \cdot 6H_2O$ in the presence of excess NEt_3 has proved to result in the formation of a neutral cluster $[(Cp^*Ir)_3(FeCl)(\mu_3\text{-}S)_4]$ (**5**) in moderate yield. Cluster **5** was allowed to react with small amount of O_2 gas to give $\mu_3\text{-}SO_2$ cluster $[(Cp^*Ir)_3(FeCl)(\mu_3\text{-}SO_2)(\mu_3\text{-}S)_3]$ (**6**). New clusters **4**, **5**, and **6** were characterized by the single crystal X-ray diffraction.

© 2010 Published by Elsevier B.V.

1. Introduction

Cubane-type (M_4S_4) metal sulfido clusters have long been attracting much attention mainly because of their close relevance to the active sites of certain metalloproteins [1]. Quite noteworthy is the mixed-metal sulfido cluster formulated as Fe_7MoS_9X ($X = C, N,$ or O) present at the active site of Mo-containing nitrogenase (FeMo-co), which consists of two corner-shared cubane-type Fe_4S_3X and Fe_3MoS_3X clusters bridged further by three $\mu_2\text{-}S$ ligands and is believed to be the site for N_2 activation and reduction (Chart 1) [2]. However, it is yet uncertain where and how N_2 molecule is bound to this cluster and converted to ammonia. Studies on the preparation of cubane-type clusters and clarifications of their reactivities toward nitrogenase substrates are therefore of much interest.

Recent research in this group has focused on the development of new reliable routes to prepare metal sulfido clusters with desired atom compositions and structures [3]. This resulted in the finding that the Ir_3 sulfido-hydrosulfido cluster $[(Cp^*Ir)_3(\mu_3\text{-}S)(\mu_2\text{-}SH)_3]Cl$ (**1**; $Cp^* = \eta^5\text{-}C_5Me_5$) prepared in this group [4] can serve as the new excellent precursor to the Ir_3MS_4 clusters of the cubane-type ($M = Sb, Bi$) or cubanoid ($M = Pd$) cores [5]. Importantly, this has led more recently to the synthesis of a series of cubane-type Ir_3RuS_4 clusters including $[(Cp^*Ir)_3\{Ru(N_2)(TMEDA)\}(\mu_3\text{-}S)_4]$ (**2**; $TMEDA = Me_2NCH_2CH_2NMe_2$)

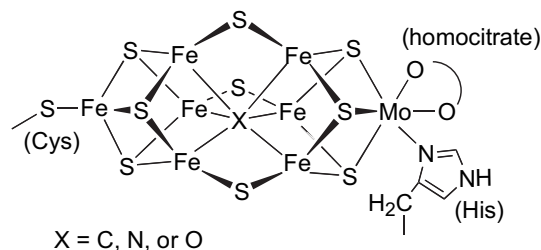**Chart 1.**

(Chart 2) [6]. It is noteworthy that **2** represents not only the first discrete metal cluster with coordinated N_2 but also the first N_2 complex with sulfido ligands that are fully characterized. The reactivities of **2** are now under investigation, which will be reported elsewhere in due course.
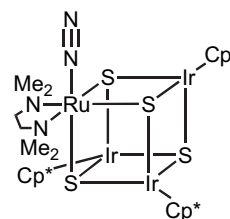

Chart 2.

* Corresponding author. Tel.: +81 3 5452 6362; Fax: +81 3 5452 6361.
  E-mail address: ymizobe@iis.u-tokyo.ac.jp (Y. Mizobe).

Now our study has been extended to the synthesis of the cubane-type clusters related to **2** containing the nitrogenase metal Fe in place of Ru, which might serve as the more excellent models of the nitrogenase active sites than **2**. In this paper we wish to describe the results of this study, viz., isolation and characterization of new cubane-type clusters containing Ir$_3$FeS$_4$ core derived from **1**.

2. Results and discussion

2.1. Preparation of Ir$_3$FeS$_4$ clusters from 1

Previously we reported the X-ray structure of the paramagnetic cubane-type cluster [(Cp*Ir)$_3$(FeCl)(μ_3-S)$_4$][FeCl$_4$] (**3**) as well as the DFT study of **3**, aiming at the evaluation of the N$_2$-binding ability of the Fe^{IV} site in the cation of **3** [7]. Single crystals of **3** for this study were obtained in quite low yield (6%) from the reaction of **1** with an equimolar amount of FeCl$_3$ in the presence of 4 equiv of NEt$_3$ in MeCN at room temperature. However, in spite of repeated attempts, isolation of **3** as pure crystals was not reproducible. On the other hand, we succeeded in the isolation of paramagnetic [(Cp*Ir)$_3$(FeCl)(μ_3-S)$_4$][FeCl$_2$(μ-Cl)$_2$FeCl$_2$]$_{0.5}$ (**4**) as single crystals in 22% yield from the reaction of **1** with 2 equiv of FeCl$_2$ in the presence of 5 equiv of NEt$_3$ in THF at room temperature (Eq. (1)). The structure of the cation [(Cp*Ir)$_3$(FeCl)(μ_3-S)$_4$]$^+$ in **4** is essentially identical with that in **3**, as demonstrated by the X-ray diffraction study (vide infra).
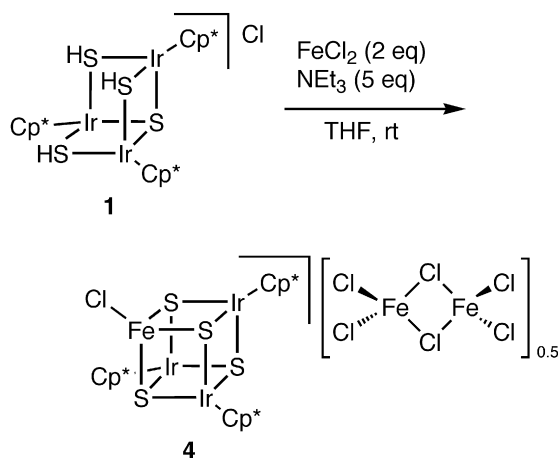
Interestingly, we have found that treatment of **1** with 2 equiv of FeCl$_3$ in the presence of 3 equiv of NEt$_3$ in THF at −60 °C, followed by stirring at room temperature, affords the neutral cluster [(Cp*Ir)$_3$(FeCl)(μ_3-S)$_4$] (**5**) containing not Fe^{IV} but Fe^{III} site in 62% yield. The reaction of **1** with one equiv of Fe(BF$_4$)$_2$·6H$_2$O and 3 equiv of NEt$_3$ in THF at −70 °C, followed by stirring of the mixture at room temperature, also proceeded to give **5** in moderate yield (Eq. (2)). Thus, it is presumed that the nature of the products, viz., cationic cluster containing Fe^{IV} or neutral one with Fe^{III}, is dependent not on the oxidation state of the Fe used as precursors but rather the reaction temperature when Fe reagents were mixed with **1**. In the absence of NEt$_3$, incorporation of Fe to the cubane-core did not take place. Paramagnetic cluster **5** was also characterized by the X-ray analysis, as described below.
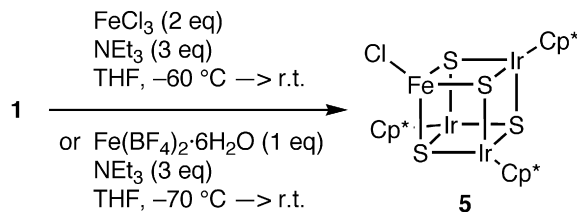
2.2. Structures of Ir$_3$FeS$_4$ clusters 4 and 5

The ORTEP drawings of **4** and **5** are shown in Figs. 1 and 2, while selected interatomic distances and angles therein are listed in Tables 1 and 2, respectively.

In the unit cell of the crystal of **4**, there exists an inversion center at the mid-point of the Fe(2)–Fe(2*) vector in the anion, and the cation and a half of the anion are crystallographically independent. The cluster has a 66-electron Ir$_3$Fe core. This somewhat electron-deficient nature, arising from the incorporation of the high-valent tetracoordinate Fe center, has resulted in the formation of Fe–Ir bonds as demonstrated by the short Fe(1)–Ir(1) distance at 2.877 (2) Å as well as the considerably shortened Fe(1)–Ir(3) distance at 2.942(1) Å, which are compatible with the presence of the metal–metal single bond for the former and some bonding interaction for the latter. The Ir–Ir separations in the range 3.56–3.61 Å are indicative of the absence of any bonding interaction between Ir centers. Due to the presence of the Fe–Ir bondings, the Ir–S bond lengths also vary, where those associated with S(3) capping the Ir$_2$Fe face with shortened Fe–Ir edges (2.313(3) and 2.326(3) Å) are shorter than the remaining Ir–S bonds (Ir–S(2) and Ir–S(4): 2.360 (3)–2.370(3); Ir–S(1): 2.386(3)–2.404(2) Å). Ignoring the metal–metal bonds, the Fe center has a distorted tetrahedral geometry with the Cl–Fe–S angles that are considerably wider than the S–Fe–S angles. The [Fe$_2$Cl$_6$]$^{2-}$ anion has the structure in good agreement with those reported previously [8]

The crystal structure of **5** has a mirror plane defined by Fe, Ir (2), S(1), and S(2) atoms. By inclusion of the Fe^{III} center, the Ir$_3$Fe core becomes less distorted as compared with that containing the
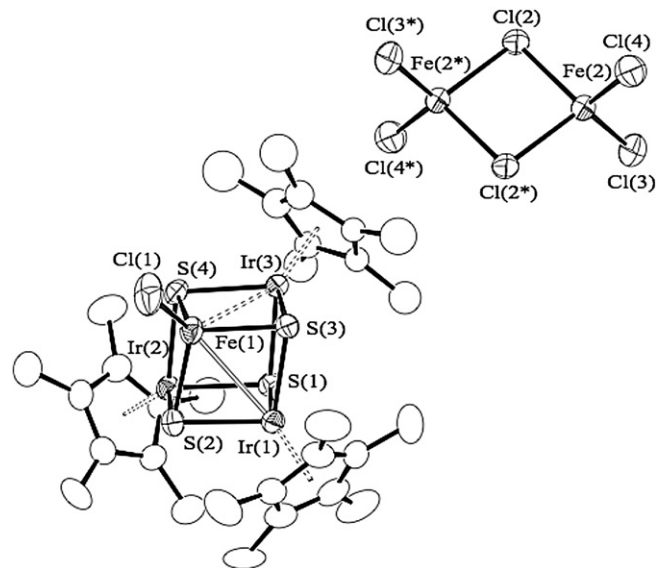

Fig. 1. An ORTEP drawing for the cation and anion in **4** at 30% probability level. All hydrogen atoms are omitted for clarity. The disordered Cp* ligand on Ir(3) with lower occupancy is also omitted.
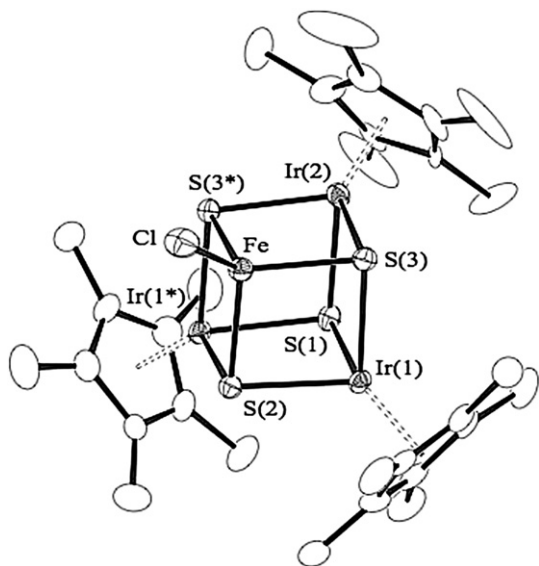
Fig. 2. An ORTEP drawing for **5** at 30% probability level. All hydrogen atoms are omitted for clarity. The disordered Cp* ligand attached to Ir(2) with lower occupancy is also omitted.

Fe^{IV} center in **4**. Thus, as shown in Table 2, the differences between two Fe–Ir, Ir–Ir, Fe–S bond distances are each quite small and the Ir–S bond lengths also fall in the small range 2.38–2.40 Å. The observed metal–metal distances (Fe–Ir: 3.127(2) and 3.071(2) Å; Ir–Ir: 3.6330(5) and 3.6167(5) Å) suggest the absence of any significant bonding interactions in this core. Around the tetrahedral Fe atom, the Cl–Fe–S angles are larger than the S–Fe–S angles.

In the related neutral cubane-type Ir(III) cluster without metal–metal bonds [(Cp*Ir)$_4$(μ_3-S)$_4$], the Ir···Ir separations are 3.602(1) and 3.584(1) Å with the Ir–S bonds in the range 2.367(3)–2.380(3) Å [9], while the core of its two-electron oxidized form [(Cp*Ir)$_4$(μ_3-S)$_4$][PF$_6$]$_2$ has one Ir–Ir bond of 2.764(1) Å together with the five Ir···Ir vectors of non-bonding distances varying from 3.563(1) to 3.683(1) Å, where the Ir–S bond lengths around the Ir–Ir bond fall in the range 2.30–2.33 Å and the others are from 2.37 to 2.41 Å [10]. In the main group metal-Ir mixed-metal cluster of the cubane-type with Ir(III)$_3$Sb(V) core, [(Cp*Ir)$_3$(SbCl$_3$)(μ_3-S)$_4$], the Ir···Ir distances are 3.579(2) and 3.556(3) Å with the Ir–S bond lengths in the range 2.333(3)–2.378(4) Å [5].

Table 1
Selected interatomic distances (Å) and angles (°) in the cation of **4**.

(a) Interatomic distances			
Fe(1)–Ir(1)	2.878(2)	Fe(1)···Ir(2)	3.128(2)
Fe(1)–Ir(3)	2.941(1)	Ir(1)···Ir(2)	3.5990(8)
Ir(1)···Ir(3)	3.5634(5)	Ir(2)···Ir(3)	3.6052(8)
Fe(1)–S(2)	2.262(3)	Fe(1)–S(3)	2.264(3)
Fe(1)–S(4)	2.277(3)	Fe(1)–Cl(1)	2.179(5)
Ir(1)–S(1)	2.395(2)	Ir(1)–S(2)	2.359(3)
Ir(1)–S(3)	2.312(3)	Ir(2)–S(1)	2.403(2)
Ir(2)–S(2)	2.364(3)	Ir(2)–S(4)	2.363(3)
Ir(3)–S(1)	2.387(3)	Ir(3)–S(3)	2.326(3)
Ir(3)–S(4)	2.369(3)		
(b) Interatomic angles			
S(2)–Fe(1)–S(3)	104.8(1)	S(2)–Fe(1)–S(4)	97.3(2)
S(2)–Fe(1)–Cl(1)	118.5(2)	S(3)–Fe(1)–S(4)	103.2(1)
S(3)–Fe(1)–Cl(1)	111.4(2)	S(4)–Fe(1)–Cl(1)	119.5(2)

Table 2
Selected interatomic distances (Å) and angles (°) in **5**.

Fe···Ir(1)	3.127(2)	Fe···Ir(2)	3.071(2)
Ir(1)···Ir(2)	3.6330(5)	Ir(1)···Ir(1*)	3.6167(5)
Fe–S(2)	2.270(4)	Fe–S(3)	2.280(2)
Fe–Cl	2.228(5)	Ir(1)–S(1)	2.387(2)
Ir(1)–S(2)	2.385(2)	Ir(1)–S(3)	2.392(2)
Ir(2)–S(1)	2.389(3)	Ir(2)–S(3)	2.396(2)
(b) Interatomic angles			
S(2)–Fe–S(3)	98.9(1)	S(2)–Fe–Cl	115.7(2)
S(3)–Fe–S(3*)	101.2(1)	S(3)–Fe–Cl	119.2(1)

2.3. Reaction of Ir$_3$FeS$_4$ cluster **5** with O$_2$

It has been found that **5** is quite air-sensitive and recrystallization from THF-ether results in the uptake of one equiv of adventitious O$_2$, affording a paramagnetic cluster [(Cp*Ir)$_3$(FeCl)(μ_3-SO$_2$)(μ_3-S)$_3$] (**6**) (eq. (3)) through the oxygenation of one sulfide ligand into the SO$_2$ ligand. Formation of **6** from **5** by treating with a small amount of O$_2$ gas in a short period was confirmed independently. Further reaction with additional amount of O$_2$ gave another species but characterization of this product was unsuccessful. The X-ray analysis has disclosed the detailed structure of **6**, in which one sulfido ligand is oxygenated to the μ_3, κ^2-SO$_2$ ligand bonded to two Ir atoms at its S atom and to the Fe atom at its one O atom (Fig. 3, Table 3). Although mono- and di-nuclear SO$_2$ complexes are well known [11], trinuclear complexes with the μ_3-SO$_2$ ligands are less common [12]. Furthermore, to the best of our knowledge, those obtained from the oxidation of their μ_3-S ligands with O$_2$ gas are yet unknown.
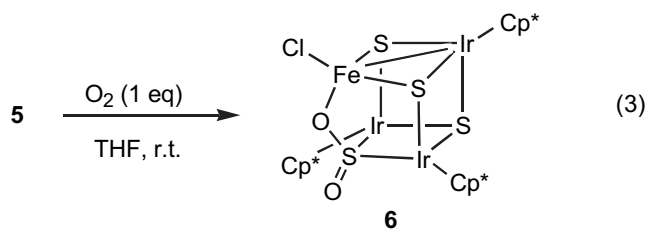

$$\textbf{5} \xrightarrow[\text{THF, r.t.}]{\text{O}_2 \text{ (1 eq)}} \textbf{6} \qquad (3)$$
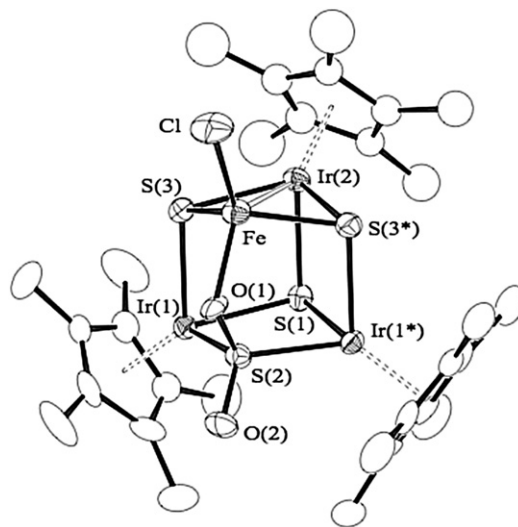

Fig. 3. An ORTEP drawing for **6** at 30% probability level. All hydrogen atoms are omitted for clarity. Only one of the two disordered Cp* groups is shown for those attached to Ir(1) and Ir(2).

Table 3
Selected interatomic distances (Å) and angles (°) in **6**.

(a) Interatomic distances			
Fe⋯Ir(1)	3.603(1)	Fe−Ir(2)	2.840(2)
Ir(1)⋯Ir(2)	3.6249(5)	Ir(1)⋯Ir(1*)	3.6078(2)
Fe−O(1)	2.002(9)	Fe−S(3)	2.284(2)
Fe−Cl	2.206(3)	Ir(1)−S(1)	2.386(2)
Ir(1)−S(2)	2.305(2)	Ir(1)−S(3)	2.370(2)
Ir(2)−S(1)	2.386(2)	Ir(2)−S(3)	2.387(2)
S(2)−O(1)	1.632(7)	S(2)−O(2)	1.462(9)
(b) Interatomic angles			
O(1)−Fe−S(3)	99.8(2)	O(1)−Fe−Cl	117.8(2)
S(3)−Fe−S(3*)	104.1(1)	S(3)−Fe−Cl	116.21(9)
Fe−O(1)−S(2)	105.2(5)	Ir(1)−S(2)−Ir(1*)	98.3(1)
Ir(1)−S(2)−O(1)	111.9(2)	Ir(1)−S(2)−O(2)	113.3(2)
O(1)−S(2)−O(2)	103.7(5)		

The Ir$_3$FeS$_4$O core in **6** is bisected by the crystallographic mirror plane passing through Ir(2), Fe, S(1), S(2), and O(1) atoms together with O(2) and Cl atoms. With respect to the Ir$_3$Fe tetrahedron, the metal−metal bond exists only between Ir(2) and Fe atoms with the distance of 2.840(2) Å and the SO$_2$ ligand caps the Ir$_2$Fe face without metal−metal bonds. In the SO$_2$ ligand, the terminal S(2)−O(2) and bridging S(2)−O(1) bond distances are 1.462(9) and 1.632(7) Å, respectively, and the O(1)−S(2)−O(2) angle is 103.7(5)°. As compared to the S−O bond length and the O−S−O angle in the parent SO$_2$ molecule at 1.431(1) Å and 119° [11c], the bridging S−O bond is elongated significantly upon coordination. The SO$_2$ ligands with the same μ$_3$, κ^2-coordination mode were observed previously in the carbonyl clusters with low-valent metal centers such as [PPN][HFe$_3$(CO)$_9$(SO$_2$)] [12a] and [PPN]$_2$[Ru$_3$(CO)$_9$(SO$_2$)] [12c] (PPN = bis(triphenylphosphine)iminium), in which the terminal S−O and bridging S−O bond distances as well as the O−S−O angles are 1.434(9) and 1.62(1) Å and 110.3(6)° for the former and 1.452(7) and 1.545(5) Å and 109.7(3)° for the latter.

Aiming coordination of N$_2$ molecule to the Fe center in the Ir$_3$FeS$_4$ core, reduction of **5** has been attempted with several reducing agents, but any tractable cluster compounds have not been obtained yet. Further derivatization of **4** and **5** is now under investigation.

3. Experimental

3.1. General

All manipulations were carried out under N$_2$ using standard Schlenk techniques. Solvents were dried by common methods and distilled under N$_2$ before use. Complex **1** was prepared according to the method described previously [4], while other chemicals were obtained commercially and used as received. The IR spectra were obtained by a JASCO FT-IR 420 spectrometer. Elemental analyses were done with a Perkin−Elmer 2400 series II CHN analyzer.

3.2. Preparation of **4**

A mixture of **1** (50 mg, 0.043 mmol), FeCl$_2$ (11 mg, 0.085 mmol), and NEt$_3$ (0.035 cm^3, 0.25 mmol) in THF (5 cm^3) was stirred at room temperature for 24 h. The resultant mixture was filtered and the dark brown filtrate was dried up in vacuo. The residue was crystallized from CH$_2$Cl$_2$−hexane, affording **4**·1.5CH$_2$Cl$_2$ as black needles (15 mg, 22% yield). Anal. Calc. for C$_{31.5}$H$_{48}$Cl$_7$Fe$_2$Ir$_3$S$_4$: C, 25.37; H, 3.24. Found: C, 24.84; H, 3.20%.

3.3. Preparation of **5**

(1) To a stirred suspension of **1** (57 mg, 0.050 mmol) in THF (5 cm^3) was added FeCl$_3$ (17 mg, 0.10 mmol) and then NEt$_3$ (0.021 cm^3,

0.15 mmol) at −60 °C. The mixture was gradually warmed to room temperature and continuously stirred over 18 h. The resultant mixture was filtered to remove colorless solid and hexane was added to the filtrate. Black crystals of **5** precipitated, which were filtered off, washed with a small portion of water, and dried in vacuo (37 mg, 62% yield).

(2) Into a mixture containing **1** (118 mg, 0.102 mmol) and Fe(BF$_4$)$_2$·6H$_2$O (35 mg, 0.10 mmol) in THF (10 cm^3) was added NEt$_3$ (0.043 cm^3, 0.31 mmol) at −70 °C. The mixture was gradually warmed to room temperature and stirred continuously for 15 h. The resultant dark solution was evaporated to dryness, the residue of which was washed with water and then dried in vacuo. The resultant solid was extracted with CH$_2$Cl$_2$ (6 cm^3) and the extract was concentrated. Addition of ether afforded **5** (57 mg, 46% yield) as black crystals. Anal. Calc. for C$_{30}$H$_{45}$ClFeIr$_3$S$_4$: C, 29.98; H, 3.77. Found: C, 30.21; H, 3.84%.

3.4. Preparation of **6**

Cluster **5** (26 mg, 0.022 mmol) was dissolved in THF and ether was layered on this solution. After 4 days, dark green crystals precipitated, which were characterized to be **6** by the X-ray analysis (13 mg, 50% yield). IR (KBr): 1100 ($\nu_{S=O}$), 794 (ν_{S-O}) cm^{-1}. Anal. Calc. for C$_{30}$H$_{45}$ClFeIr$_3$O$_2$S$_4$ requires C, 29.20; H, 3.68. Found: C, 29.33; H, 3.54%. Formation of **6** by exposure of the THF solution of **5** to air for a few minutes has been confirmed by recording the IR spectrum of the evaporated reaction mixture residue, which showed the ν(S=O) and ν(S−O) bands characteristic to **6**. However, isolation of pure **6** from this reaction mixture was unsuccessful.

3.5. X-ray crystallography

Single crystals of **4**·CH$_2$Cl$_2$, **5** and **6** were sealed in glass capillaries under argon and mounted on a Rigaku AFC-7R four-circled diffractometer (for **4**) or a Mercury-CCD diffractometer (for **5** and **6**), equipped with a graphite-monochromatized Mo-Kα source. All diffraction studies were done at 23 °C, whose details are listed in Table 4. Data collection was performed by the use of the WinAFC

Table 4
Details of X-ray crystallography for **4**·1.5CH$_2$Cl$_2$, **5** and **6**.

	4·1.5CH$_2$Cl$_2$	**5**	**6**
Formula	C$_{31.5}$H$_{48}$Cl$_7$Fe$_2$Ir$_3$S$_4$	C$_{30}$H$_{45}$ClFeIr$_3$S$_4$	C$_{30}$H$_{45}$ClFeIr$_3$O$_2$S$_4$
Formula weight	1491.49	1201.89	1233.88
Crystal system	Triclinic	Monoclinic	Orthorhombic
Space group	P$\bar{1}$(No. 2)	P2$_1$/m (No. 11)	Cmca (No. 64)
a (Å)	13.212(7)	9.923(4)	18.157(4)
b (Å)	13.60(1)	18.296(6)	17.528(4)
c (Å)	14.768(5)	9.847(3)	22.760(5)
α (°)	78.01(4)	90	90
β (°)	81.22(4)	100.463(5)	90
γ (°)	61.47(5)	90	90
V (Å^3)	2276(2)	1758(1)	7244(3)
Z	2	2	8
ρ_{calcd} (g cm^{-3})	2.176	2.270	2.263
μ (mm^{-1})	9.999	12.087	11.741
Crystal size (mm^3)	0.40 × 0.40 × 0.30	0.20 × 0.20 × 0.03	0.30 × 0.30 × 0.10
No. of unique reflns	10 419	4137	4285
no. of data with I > 2σ(I)	6375	2399	2611
No. of variables	462	224	231
Transmn factor	0.039−0.051	0.247−0.696	0.102−0.309
R1[a]	0.045	0.040	0.035
wR2[b]	0.138	0.134	0.118
GOF[c]	1.039	1.004	1.043

[a] R1 = Σ||F$_0$| − |F$_c$||/Σ|F$_0$| (I > 2σ(I)).
[b] wR2 = [Σ(w(F$_0^2$ − F$_c^2$)^2)/Σw(F$_0^2$)^2]$^{1/2}$ (all data).
[c] GOF = [Σw(|F$_0$| − |F$_c$|)^2/{(no. observed) − (no. variables)}]$^{1/2}$.

(for **4**) or the CrystalClear program package (for **5** and **6**) [13]. All data were corrected for absorption. Structure solution and refinements were conducted by using the CrystalStructure program package [14]. The positions of non-hydrogen atoms were determined by Patterson methods (PATTY) [15] and subsequent Fourier synthesis (DIRDIF99) [16], which were refined by full-matrix least-squares techniques.

Acknowledgements

Appendix A. Supplementary material

CCDC 768215, 768 216 and 768 217 contain the supplementary crystallographic data for **4**·1.5CH$_2$Cl$_2$, **5** and **6**. These data can be obtained free of charge from The Cambridge Crystallographic Data Centre via www.ccdc.cam.ac.uk/data_request/cif.

References

[1] (a) Y. Mizobe, in: F.A. Devillanova (Ed.), Handbook of Chalcogen Chemistry, RSC Pubishing, Cambridge, UK, 2007, pp. 725–741 Chapter. 11.2;
(b) S.C. Lee, R.H. Holm, Chem. Rev. 104 (2004) 1135;
(c) R. Hernandez-Molina, M.N. Sokolov, A.G. Sykes, Acc. Chem. Res. 34 (2001) 223;
(d) T. Shibahara, Adv. Inorg. Chem. 37 (1991) 143;
(e) K. Herbst, P. Zanello, M. Corsini, N. D'Amelio, L. Dahlenburg, M. Brorson, Inorg. Chem. 42 (2003) 974;
(f) I. Takei, K. Kobayashi, K. Dohki, S. Nagao, Y. Mizobe, M. Hidai, Chem. Lett. 36 (2007) 546.

[2] O. Einsle, F.A. Tezcan, S.L.A. Andrade, B. Schmid, M. Yoshida, J.B. Howard, D.C. Rees, Science 297 (2002) 1696.
[3] (a) M. Hidai, Y. Mizobe, Can. J. Chem. 83 (2005) 358;
(b) M. Hidai, S. Kuwata, Y. Mizobe, Acc. Chem. Res. 33 (2000) 46.
[4] F. Takagi, H. Seino, Y. Mizobe, M. Hidai, Organometallics 21 (2002) 694.
[5] A. Shinozaki, H. Seino, M. Hidai, Y. Mizobe, Organometallics 22 (2003) 5636.
[6] (a) H. Mori, H. Seino, M. Hidai, Y. Mizobe, Angew. Chem. Int. Ed. 46 (2007) 5431;
(b) H. Tanaka, H. Mori, H. Seino, M. Hidai, Y. Mizobe, K. Yoshizawa, J. Am. Chem. Soc. 130 (2008) 9037.
[7] (a) P.M. Kozlowski, Y. Shiota, S. Gomita, H. Seino, Y. Mizobe, K. Yoshizawa, Bull. Chem. Soc. Jpn. 80 (2007) 2323;
(b) H. Tanaka, F. Ohsako, H. Seino, Y. Mizobe, K. Yoshizawa, Inorg. Chem 49 (2010) 2464.
[8] (a) J.-S. Sun, H. Zhao, X. Ouyang, R. Clérac, J.A. Smith, J.M. Clemente-Juan, C. Gómez-Garcia, E. Coronado, K.R. Dunbar, Inorg. Chem. 38 (1999) 5841;
(b) K.R. Dunbar, A. Quillevéré, Amgew. Chem. Int. Ed. Engl. 32 (1993) 293.
[9] D.A. Dobbs, R.G. Bergman, Inorg. Chem. 33 (1994) 5329.
[10] A. Venturelli, T.B. Rauchfuss, J. Am. Chem. Soc. 116 (1994) 4824.
[11] (a) W.A. Schenk, Angew. Chem. Int. Ed. Engl. 26 (1987) 98;
(b) R.R. Ryan, G.J. Kubas, D.C. Moody, P.G. Eller, Structure and Bonding 46 (1981) 47;
(c) D.M.P. Mingos, Transition Met. Chem. 3 (1978) 1.
[12] (a) G.B. Karet, C.L. Stern, D.M. Norton, D.F. Shriver, J. Am. Chem. Soc. 115 (1993) 9979;
(b) R.W. Eveland, C.C. Raymond, T.E. Albrecht-Schmitt, D.F. Shriver, Inorg. Chem. 38 (1999) 1282;
(c) G.B. Karet, C.L. Stern, J.A. Cody, S.J. Lange, M.A. Pell, C. Slebodnick, D. F. Shriver, J. Organomet. Chem. 495 (1995) 33.
[13] CRYSTALCLEAR 1.3.5 Rigaku and Rigaku/MSC, 1998–2006; J.W. Pflugrath Acta Cryst. D 55 1999 1718
[14] J.R. Carruthers, J.S. Rollett, P.W. Betteridge, D. Kinna, L. Pearce, A. Larsen, E. Gabe, CRYSTALSTRUCTURE 3.8.0: Crystal Structure Analysis Package, Rigaku and Rigaku/MSC: New Trails Dr., The Woodlands, TX 77381, USA, 2000–2006; CRYSTALS Issue 11. Chemical Crystallography Laboratory, Oxford, UK, 1999.
[15] PATTY P.T. Beurskens, G. Admiraal, G. Beurskens, W.P. Bosman, S. Garcia-Granda, R.O. Gould, J.M.M. Smits, C. Smykall, The DIRDIF Program System, Technical Report of the Crystallography Laboratory. University of Nijmegen, The Netherlands, 1992.
[16] DIRDIF-99 P.T. Beurskens, G. Admiraal, G. Beurskens, W.P. Bosman, R. de Gelder, R. Israel, J.M.M. Smits, The DIRDIF-99 Program System, Technical Report of the Crystallography Laboratory. University of Nijmegen, The Netherlands, 1999.